

000  
001  
002054  
055  
056

# Multi-channel Weighted Nuclear Norm Minimization for Real Color Image Denoising

057  
058  
059003  
004  
005  
006  
007060  
061  
062  
063

Anonymous ICCV submission

008  
009  
010  
011  
012064  
065  
066

Paper ID 572

013  
014  
015067  
068  
069

## Abstract

The noise structures among the R, G, B channels of real images are quite different due to the preprocessing steps, such as demosaicing, white balance, etc., of the in-camera imaging pipelines. This makes the real image denoising problem much more complex than traditional grayscale image denoising. In this paper, we propose a multi-channel optimization model for real color image denoising. Specifically, we introduce a weighting matrix into the data term to process adaptively each part of R, G, B channels in the joint patches concatenated by corresponding patches in these channels. In the regularization term, we employ the weighted nuclear norm to exploit the non-local self similar property. The proposed multi-channel weighted nuclear norm minimization (WNNM) model is much more complex than the standard WNNM model. We reformulate the proposed model into a linear equality-constrained optimization problem and solve it by the alternating direction method of multipliers algorithm. Each alternative updating step has closed-form solution and the convergence results are given. Experiments on benchmark datasets demonstrate that the proposed model outperforms state-of-the-art denoising methods on synthetic as well as real-world noisy images.

lent denoising performance by exploiting the NSS property via low rank regularization.

The real color image denoising problem is not a trivial extension from single channel (grayscale image) to multiple channels (color image). The reason is that the noise structures are quite different among the Red (R), Green (G), Blue (B) channels of images captured by CCD or CMOS cameras due to the on-board processing steps [13]. This makes the real color image denoising problem much more complex. Directly applying the denoising methods for grayscale images to each channel of color images separately would obtain bad performance [14]. There are several work [14–19] proposed specifically for color image denoising. The method [15] first transforms the color images into the luminance/chrominance space such as YCbCr before denoising, but this would make the noise distribution more complex in color images. The methods of [14, 19] process the joint patches concatenated by the corresponding patches in R, G, B channels and treat equally the patches in different channels. This would generate false colors or artifacts [14]. The methods of [16–18] ignore the non-local self similarity property of natural images, and their performance would be largely depressed [2, 7].

In order to deal with the R, G, B channels in color images more effectively, different noise properties of different channels should be considered in solving real color image denoising problem. Besides, due to its expressive denoising performance, the WNNM model [7] is employed to exploit the NSS property of natural images. In this paper, we proposed a multi-channel WNNM model for real color image denoising. By introducing a weighting matrix to the WNNM model, the proposed multi-channel WNNM model no longer has closed-form solutions and more challenging to solve. By reformulating the proposed multi-channel WNNM model into a linear equality-constrained program with two variables, the relaxed problem can be solved under the alternating direction method of multipliers (ADMM) [20] framework. Each variable can be updated with closed-form solution [7, 21]. We also give the convergency results with detailed proof to guarantee a rational termination of

## 1. Introduction

Image denoising is an important problem in enhancing the image quality in computer vision systems. The traditional grayscale image denoising problem aims to recover the clean image  $\mathbf{x}$  from the noisy observation  $\mathbf{y} = \mathbf{x} + \mathbf{n}$ , where  $\mathbf{n}$  is often assumed to be additive white Gaussian noise (AWGN). Most image denoising methods in this field either employ the non-local self similarity (NSS) of natural images [1–7] or learn generative or discriminative denoisers from paired natural clean images and synthetic noisy images [8–12]. Among these methods, the weighted nuclear norm minimization (WNNM) method achieves exal-

108  
109  
110  
111  
112  
113  
114  
115  
116  
117  
118  
119  
120  
121  
122  
123  
124  
125  
126  
127  
128  
129  
130  
131  
132  
133  
134  
135  
136  
137  
138  
139  
140  
141  
142  
143  
144  
145  
146  
147  
148  
149  
150  
151  
152  
153  
154  
155  
156  
157  
158  
159  
160  
161

the proposed algorithm.

## 2. Related Work

### 2.1. Weighted Nuclear Norm Minimization

As an extension to the nuclear norm minimization (NNM) model [22], the weighted nuclear norm minimization (WNNM) model [7] is described as

$$\min_{\mathbf{X}} \|\mathbf{Y} - \mathbf{X}\|_F^2 + \|\mathbf{X}\|_{w,*} \quad (1)$$

where  $\|\mathbf{X}\|_{w,*} = \sum_i w_i \sigma_i(\mathbf{X})$  is the weighted nuclear norm of matrix  $\mathbf{X}$ , and  $\mathbf{w} = [w_1, \dots, w_n]^\top$ ,  $w_i \geq 0$  is the weight vector,  $\sigma_i(\mathbf{X})$  is the  $i$ -th singular value of matrix  $\mathbf{X}$ . According to the Corollary 1 of [23], the problem (1) has closed-form solution if the weights are non-decreasing

$$\hat{\mathbf{X}} = \mathbf{U} \mathcal{S}_{w/2}(\Sigma) \mathbf{V}^\top \quad (2)$$

where  $\mathbf{Y} = \mathbf{U} \Sigma \mathbf{V}^\top$  is the singular value decomposition [24] of  $\mathbf{Y}$  and  $\mathcal{S}_\tau(\bullet)$  is the generalized soft-thresholding operator with weight vector  $\mathbf{w}$ :

$$\mathcal{S}_{w/2}(\Sigma_{ii}) = \max(\Sigma_{ii} - w_{ii}/2, 0) \quad (3)$$

Though having achieved excellent performance on grayscale image denoising, the WNNM model would generate false colors or artifacts [14], if being directly extended to real color image denoising by processing each channel separately or joint vectors concatenated by multiple channels. In this paper, for real noisy image denoising, we propose a multi-channel WNNM model which preserve the power of WNNM and be able to process the differences among different channels.

### 2.2. Real Color Image Denoising

During the last decade, several denoising methods are proposed for real color image denoising [15–17, 19]. Among them, the CBM3D [15] first transform the RGB image into luminance-chrominance space (e.g., YCbCr) and then apply the famous BM3D method [2] on each channel separately with the patches being grouped only in the luminance channel. In [16], the authors proposed the “Noise Level Function” to estimate and remove the noise for each channel in natural images. However, the methods processing each channel separately would achieve inferior performance than processing jointly these channels [14]. The methods of [17, 19, 25] perform real color image denoising by concatenating the patches in R, G, B channels into joint vectors. However, the concatenation would treat each channel equally and ignore the different noise properties among these channels. The method in [18] models the cross-channel noise in real noisy image as a multivariate Gaussian and the noise is removed by the Bayesian non-local means filter [26]. The commercial software Neat Image [27] estimates the noise parameters from a flat region of the given noisy image and filters the noise correspondingly. But these methods [18, 27] ignore the non-local self similarity property of natural images [2, 7].

In this paper, we introduce a weighting matrix which add different weights to different channels for color image denoising. The proposed multi-channel method can effectively solve the problem of different noise structures among different channels.

162  
163  
164  
165  
166  
167  
168  
169  
170  
171  
172  
173  
174  
175  
176  
177  
178  
179  
180  
181  
182  
183  
184  
185  
186  
187  
188  
189  
190  
191  
192  
193  
194  
195  
196  
197  
198  
199  
200  
201  
202  
203  
204  
205  
206  
207  
208  
209  
210  
211  
212  
213  
214  
215

## 3. Color Image Denoising via Multi-channel Weighted Nuclear Norm Minimization

### 3.1. The Problem

The color image denoising problem is to recover the clean image  $\{\mathbf{x}_c\}$  from its noisy version  $\mathbf{y}_c = \mathbf{x}_c + \mathbf{n}_c$ , where  $c \in \{r, g, b\}$  is the index of R, G, B channels and  $\mathbf{n}_c$  is the noise in  $c$ -th channel. The noise structures in each channel are different due to the on-board processing of the in-camera imaging pipeline [13]. Therefore, it is problematic to directly apply denoising methods to the joint vectors concatenated by corresponding patches of the R, G, B channels. To validate this point, in Fig. 1, we show the clean image “kodim23” taken from the Kodak PhotoCD dataset, its degraded version generated by adding synthetic additive white Gaussian noise (AWGN) to each channel of “kodim23”, and the denoised image by applying WNNM [7] on the joint vectors concatenated from R, G, B channels of the degraded image. The standard derivations of AWGN added to the R, G, B channels are  $\sigma_r = 40$ ,  $\sigma_g = 20$ ,  $\sigma_b = 30$ , respectively. The input standard derivation of the noise for the concatenated WNNM method is set as the Root Mean Square (RMS) of those in each channel, i.e.,  $\sigma = \sqrt{(\sigma_r^2 + \sigma_g^2 + \sigma_b^2)/3} = 31.1$ . From Fig. 1, one can see that the concatenated WNNM method treating each channel equally would remain some noise in the R and B channel, while oversmoothing the G channel of the degraded image. Hence, if the patches of different channels are treated adaptively in the concatenated vectors, the degraded color images would be recovered with better visual qualities.

In order to process each channel differently while still exploiting the joint structures of the color images, in this paper, we introduce a weighting matrix  $\mathbf{W}$  to the concatenated WNNM method. Assume the matrix  $\mathbf{Y}$  containing the noisy patches in R, G, B channels as  $\mathbf{Y} = [\mathbf{Y}_r^\top \mathbf{Y}_g^\top \mathbf{Y}_b^\top]^\top$ , the corresponding clean matrix  $\mathbf{X} = [\mathbf{X}_r^\top \mathbf{X}_g^\top \mathbf{X}_b^\top]^\top$ , and the weights  $\mathbf{w}$  for the singular values of  $\mathbf{X}$ , then the proposed multi-channel WNNM (MC-WNNM) model is

$$\min_{\mathbf{X}} \|\mathbf{W}(\mathbf{Y} - \mathbf{X})\|_F^2 + \|\mathbf{X}\|_{w,*..} \quad (4)$$

How to set the weighting matrix  $\mathbf{W}$  and how to solve the proposed model will be introduced in the next sections.

### 3.2. The Setting of Weighting Matrix $\mathbf{W}$

For simplicity, in this paper, we assume the noise are independent among the R, G, B channels and i.i.d. in each

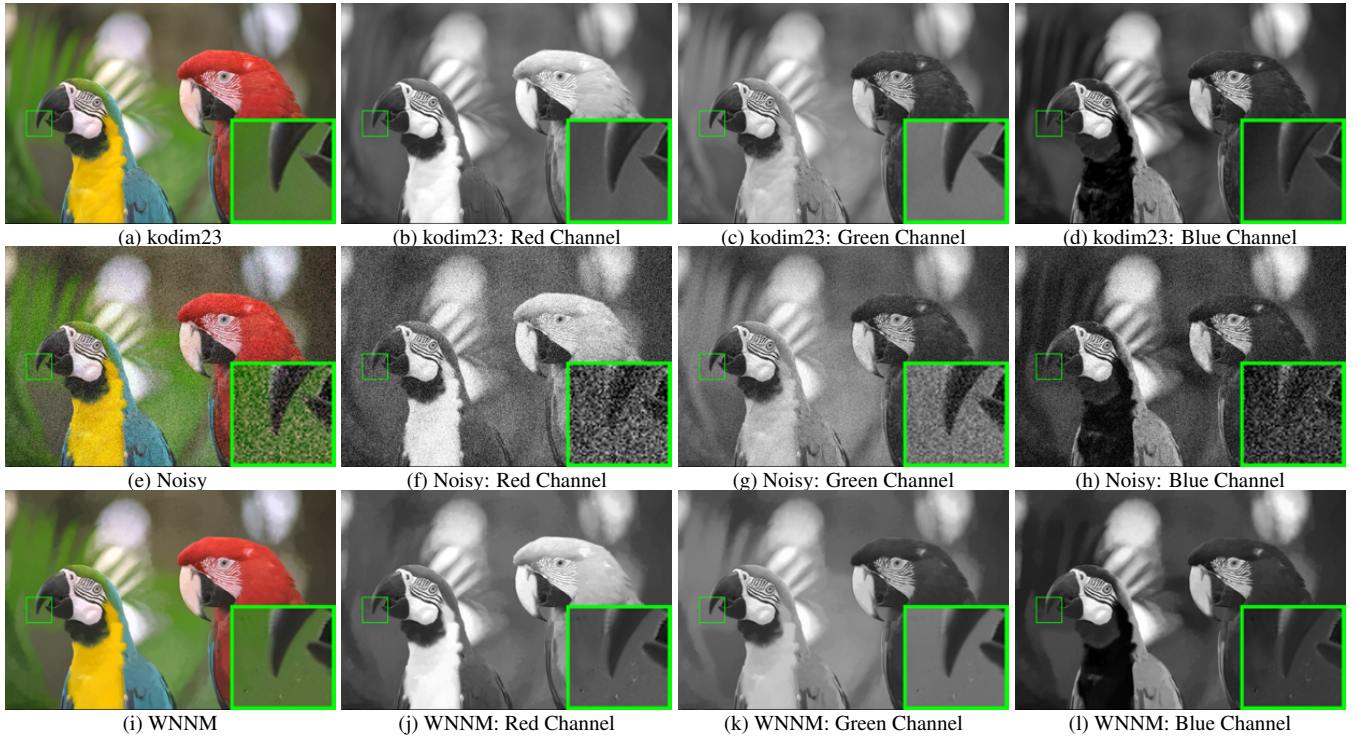


Figure 1. The image “kodim23” of the Kodak PhotoCD dataset, its degraded version, and the image recovered by WNNM. The R, G, B channels are also listed here for image quality comparison.

channel. Therefore, the weighting matrix  $\mathbf{W}$  is diagonal and can be determined under the Bayesian framework:

$$\begin{aligned} \hat{\mathbf{X}} &= \arg \max_{\mathbf{X}} \ln P(\mathbf{X}|\mathbf{Y}, \mathbf{w}) \\ &= \arg \max_{\mathbf{X}} \{ \ln P(\mathbf{Y}|\mathbf{X}) + \ln P(\mathbf{X}|\mathbf{w}) \}. \end{aligned} \quad (5)$$

The log-likelihood term  $\ln P(\mathbf{Y}|\mathbf{X})$  is characterized by the statistics of noise, which is assumed to be channel-wise independent white Gaussian with standard deviations  $\{\sigma_r, \sigma_g, \sigma_b\}$

$$P(\mathbf{Y}|\mathbf{X}) = \prod_{c \in \{r,g,b\}} (2\pi\sigma_c^2)^{-\frac{3p^2}{2}} \exp\left(-\frac{1}{2\sigma_c^2} \|\mathbf{Y}_c - \mathbf{X}_c\|_F^2\right). \quad (6)$$

We assume that the matrix  $\mathbf{X}$  follows the following distribution

$$P(\mathbf{X}|\mathbf{w}) \propto \exp\left(-\frac{1}{2} \|\mathbf{X}\|_{\mathbf{w},*}\right). \quad (7)$$

Putting (7) and (6) into (5), we have

$$\hat{\mathbf{X}} = \arg \min_{\mathbf{X}} \|\mathbf{W}(\mathbf{Y} - \mathbf{X})\|_F^2 + \|\mathbf{X}\|_{\mathbf{w},*}, \quad (8)$$

where

$$\mathbf{W} = \begin{pmatrix} \sigma_r^{-1} \mathbf{I} & \mathbf{0} & \mathbf{0} \\ \mathbf{0} & \sigma_g^{-1} \mathbf{I} & \mathbf{0} \\ \mathbf{0} & \mathbf{0} & \sigma_b^{-1} \mathbf{I} \end{pmatrix}. \quad (9)$$

where  $\mathbf{I} \in \mathbb{R}^{p^2 \times p^2}$  is the identity matrix. Hence, the weighting matrix  $\mathbf{W}$  is determined to contribute equal weights for the pixel values in the same channel, while different weights for those in different channels. The experimental (which will be introduced later) results have already demonstrated

that this form of weighting matrix have already generated the best denoising performance on synthetic and real noisy images in benchmark datasets.

### 3.3. The Denoising Algorithm

In this section, with the proposed MC-WNNM model, we propose a denoising algorithm for color images. In our algorithm, given a noisy image  $\mathbf{y}$ , each local patch is extracted from it with patch size  $p \times p \times 3$  and stretched to a patch vector  $\mathbf{y}_j \in \mathbb{R}^{3p^2}$  concatenated by corresponding patches in R, G, B, channels. Then we search the  $M$  most similar patches to  $\mathbf{y}_j$  (including  $\mathbf{y}_j$  itself) by Euclidean distance in a  $W \times W$  local region around it. We stack the  $M$  similar patches column by column to form a noisy patch matrix  $\mathbf{Y}_j = \mathbf{X}_j + \mathbf{N}_j \in \mathbb{R}^{3p^2 \times M}$ , where  $\mathbf{X}_j$  and  $\mathbf{N}_j$  the corresponding clean and noise patch matrices. Then, we can apply the proposed MC-WNNM model to  $\mathbf{Y}_j$  to estimate  $\hat{\mathbf{X}}_j$  for color image denoising:

$$\min_{\mathbf{X}_j} \|\mathbf{W}_j(\mathbf{Y}_j - \mathbf{X}_j)\|_F^2 + \|\mathbf{X}_j\|_{\mathbf{w},*}. \quad (10)$$

where  $\mathbf{W}_j$  is defined in Eq. (9). Just as [23] did, the weight vector  $\mathbf{w}$  is set  $w_i^{k+1} = \frac{C}{|\sigma_i(\mathbf{X}_k)| + \epsilon}$  and  $\epsilon > 0$  is a small number to avoid zero numerator. Note that when  $\sigma_r = \sigma_g = \sigma_b$ , the multi-channel WNNM model will be reduced to the concatenated WNNM model as a special case.

The multi-channel WNNM is applied to the noisy patch matrix  $\mathbf{Y}_j$  of each local patch  $\mathbf{y}_j$  in the noisy image  $\mathbf{y}$ . And

324  
 325   **Algorithm 1:** Color Image Denoising by MC-WNNM  
 326   **Input:** Noisy image  $\mathbf{y}$ , noise levels  $\{\sigma_r, \sigma_g, \sigma_b\}$ ;  
 327   **Initialization:**  $\hat{\mathbf{x}}^{(0)} = \mathbf{y}, \mathbf{y}^{(0)} = \mathbf{y}$ ;  
 328   **for**  $k = 1 : K_1$  **do**  
 329     1. Set  $\mathbf{y}^{(k)} = \hat{\mathbf{x}}^{(k-1)}$ ;  
 330     2. Extracte local patches  $\{\mathbf{y}_j\}_{j=1}^N$  from  $\mathbf{y}^{(k)}$ ;  
 331       **for** each patch  $\mathbf{y}_j$  **do**  
 332         3. Search non-local similar patches  $\mathbf{Y}_j$ ;  
 333         4. Applying the MC-WNNM model (10) to  $\mathbf{Y}_j$  and  
 334           obtain the estimated  $\mathbf{X}_j$ ;  
 335       **end for**  
 336     5. Aggregate  $\{\mathbf{X}_j\}_{j=1}^N$  to form the image  $\hat{\mathbf{x}}^{(k)}$ ;  
 337   **end for**  
 338   **Output:** Denoised image  $\hat{\mathbf{x}}^{K_1}$ .

339 then all the patches are aggregated together to form the final  
 340 recovered image  $\hat{\mathbf{y}}$ . To obtain better denoising results,  
 341 we perform the above denoising procedure for several ( $K_1$ )  
 342 iterations. The proposed MC-WNNM denoising algorithm  
 343 for color images is summarized in Algorithm 1.

### 3.4. Optimization

344 The proposed MC-WNNM model could not be solved  
 345 in an analytical form while the original WNNM model  
 346 [23] could. In the WNNM model, when the weights on  
 347 singular values are non-descending, the weighted nuclear  
 348 norm proximal operator [23] can have global optimum with  
 349 closed-form solution. However, such property is not valid  
 350 for the multi-channel WNNM model. The reason is that the  
 351 weighting matrix  $\mathbf{W}$  is added to the rows of matrix  $\mathbf{X}$  instead  
 352 of its singular values. Besides, the elements in  $\mathbf{W}$  is  
 353 not in a non-descending order with respect to the singular  
 354 value of  $\mathbf{X}$ . This makes the proposed model more difficult  
 355 to solve when compared to the original WNNM model.

356 By introducing an augmented variable  $\mathbf{Z}$ , the MC-  
 357 WNNM model is reformulated as a linear equality-  
 358 constrained problem with two variables  $\mathbf{X}$  and  $\mathbf{Z}$ :

$$359 \min_{\mathbf{X}, \mathbf{Z}} \|\mathbf{W}(\mathbf{Y} - \mathbf{X})\|_F^2 + \|\mathbf{Z}\|_{w,*} \quad \text{s.t. } \mathbf{X} = \mathbf{Z}. \quad (11)$$

360 Since the objective function is separable across the two variables,  
 361 the problem (11) can be solved by under alternating direction method of multipliers (ADMM) framework. We  
 362 can derive its augmented Lagrangian function:

$$363 \mathcal{L}(\mathbf{X}, \mathbf{Z}, \mathbf{A}, \rho) = \|\mathbf{W}(\mathbf{Y} - \mathbf{X})\|_F^2 + \|\mathbf{Z}\|_{w,*} \\ 364 + \langle \mathbf{A}, \mathbf{X} - \mathbf{Z} \rangle + \frac{\rho}{2} \|\mathbf{X} - \mathbf{Z}\|_F^2 \quad (12)$$

365 where  $\mathbf{A}$  is the augmented Lagrangian multiplier and  $\rho > 0$   
 366 is the penalty parameter. We initialize the matrix variables  
 367  $\mathbf{X}_0, \mathbf{Z}_0$ , and  $\mathbf{A}_0$  to be zero matrix of suitable size. By taking  
 368 derivative of the Lagrangian function  $\mathcal{L}$  with respect to the  
 369 variables  $\mathbf{X}$  and  $\mathbf{Z}$  and setting the derivative function to be zero, we can alternatively update the ADMM algorithm  
 370 iteratively as follows:  
 371 (1) **Update X while fixing Z and A:**

$$372 \mathbf{X}_{k+1} = \arg \min_{\mathbf{X}} \|\mathbf{W}(\mathbf{Y} - \mathbf{X})\|_F^2 + \frac{\rho_k}{2} \|\mathbf{X} - \mathbf{Z}_k + \rho_k^{-1} \mathbf{A}_k\|_F^2 \quad (13)$$

373 This is a least squares regression problem with closed-form  
 374 solution:  
 375

$$376 \mathbf{X}_{k+1} = (\mathbf{W}^\top \mathbf{W} + \frac{\rho_k}{2} \mathbf{I})^{-1} (\mathbf{W}^\top \mathbf{W} \mathbf{Y} + \frac{\rho_k}{2} \mathbf{Z}_k - \frac{1}{2} \mathbf{A}_k) \quad (14)$$

377 (2) **Update Z while fixing X and A:**

$$378 \mathbf{Z}_{k+1} = \arg \min_{\mathbf{Z}} \frac{\rho_k}{2} \|\mathbf{Z} - (\mathbf{X}_{k+1} + \rho_k^{-1} \mathbf{A}_k)\|_F^2 + \|\mathbf{Z}\|_{w,*} \quad (15)$$

379 According to the Theorem 1 in [23], given the  $\mathbf{X}_{k+1} + \rho_k^{-1} \mathbf{A}_k = \mathbf{U}_k \Sigma_k \mathbf{V}_k^\top$  be the SVD of  $\mathbf{X}_{k+1} + \rho_k^{-1} \mathbf{A}_k$ ,  
 380 where  $\Sigma_k = \begin{pmatrix} \text{diag}(\sigma_1, \sigma_2, \dots, \sigma_n) \\ \mathbf{0} \end{pmatrix} \in \mathbb{R}^{m \times n}$ , then the  
 381 global optimum of the above problem is  $\hat{\mathbf{Z}} = \mathbf{U}_k \hat{\Sigma}_k \mathbf{V}_k^\top$ ,  
 382 where  $\hat{\Sigma}_k = \begin{pmatrix} \text{diag}(\hat{\sigma}_1, \hat{\sigma}_2, \dots, \hat{\sigma}_n) \\ \mathbf{0} \end{pmatrix} \in \mathbb{R}^{m \times n}$  and  
 383  $(\hat{\sigma}_1, \hat{\sigma}_2, \dots, \hat{\sigma}_n)$  is the solution to the following convex optimization problem:

$$384 \min_{\hat{\sigma}_1, \hat{\sigma}_2, \dots, \hat{\sigma}_n} \sum_{i=1}^n (\sigma_i - \hat{\sigma}_i)^2 + \frac{2w_i}{\rho_k} \hat{\sigma}_i \quad (16)$$

385 s.t.  $\hat{\sigma}_1 \geq \hat{\sigma}_2 \geq \dots \geq \hat{\sigma}_n \geq 0$ .

386 According to the Remark 1 in [23], the problem above has  
 387 closed-form solution

$$388 \hat{\sigma}_i = \begin{cases} 0 & \text{if } c_2 < 0 \\ \frac{c_1 + \sqrt{c_2}}{2} & \text{if } c_2 \geq 0 \end{cases} \quad (17)$$

389 where  $c_1 = \sigma_i - \epsilon$ ,  $c_2 = (\sigma_i - \epsilon)^2 - \frac{8C}{\rho_k}$  and  $C$  is set as  
 390  $\sqrt{2n}$  by experience in image denoising.

391 (3) **Update A while fixing X and Z:**

$$392 \mathbf{A}_{k+1} = \mathbf{A}_k + \rho_k (\mathbf{X}_{k+1} - \mathbf{Z}_{k+1}) \quad (18)$$

393 (4) **Update  $\rho_k$ :**  $\rho_{k+1} = \mu * \rho_k$ , where  $\mu > 1$ .

394 The above alternative updating steps are repeated until  
 395 the convergence condition is satisfied or the number of  
 396 iterations exceeds a preset maximum number, e.g.,  $K_2$ .  
 397 The convergence condition of the ADMM algorithm is:  
 398  $\|\mathbf{X}_{k+1} - \mathbf{Z}_{k+1}\|_F \leq \text{Tol}$ ,  $\|\mathbf{X}_{k+1} - \mathbf{X}_k\|_F \leq \text{Tol}$ , and  
 399  $\|\mathbf{Z}_{k+1} - \mathbf{Z}_k\|_F \leq \text{Tol}$  are simultaneously satisfied, where  
 400  $\text{Tol} > 0$  is a small tolerance. We summarize the optimization  
 401 steps in Algorithm 2. The convergence analysis of the  
 402 proposed Algorithm 2 is given in Theorem 1. Note that  
 403 since the weighted nuclear norm is non-convex in general,  
 404 we employ an unbounded sequence of  $\{\rho_k\}$  here to make  
 405 sure that the Algorithm 2 is convergent.

406 **Theorem 1.** Assume the weights in  $w$  are in a non-  
 407 descending order, the sequence  $\{\mathbf{X}_k\}$ ,  $\{\mathbf{Z}_k\}$ , and  $\{\mathbf{A}_k\}$   
 408 generated in Algorithm 1 satisfy:

$$409 (a) \lim_{k \rightarrow \infty} \|\mathbf{X}_{k+1} - \mathbf{Z}_{k+1}\|_F = 0; \quad (19)$$

$$410 (b) \lim_{k \rightarrow \infty} \|\mathbf{X}_{k+1} - \mathbf{X}_k\|_F = 0; \quad (20)$$

$$411 (c) \lim_{k \rightarrow \infty} \|\mathbf{Z}_{k+1} - \mathbf{Z}_k\|_F = 0. \quad (21)$$

432	<b>Algorithm 2:</b> Solve MC-WNNM via ADMM	486
433	<b>Input:</b> Matrices $\mathbf{Y}$ and $\mathbf{W}$ , $\mu > 1$ , $\text{Tol} > 0$ ;	487
434	<b>Initialization:</b> $\mathbf{X}_0 = \mathbf{Z}_0 = \mathbf{A}_0 = \mathbf{0}$ , $\rho_0 > 0$ , $\text{T} = \text{False}$ ,	488
435	$k = 0$ ;	489
436	<b>While</b> ( $\text{T} == \text{false}$ ) <b>do</b>	490
437	1. Update $\mathbf{X}_{k+1}$ as	491
438	$\mathbf{X}_{k+1} = (\mathbf{W}^\top \mathbf{W} + \frac{\rho_k}{2} \mathbf{I})^{-1} (\mathbf{W}^\top \mathbf{W} \mathbf{Y} + \frac{\rho_k}{2} \mathbf{Z}_k - \frac{1}{2} \mathbf{A}_k)$	492
439	2. Update $\mathbf{Z}_{k+1}$ by solving the problem	493
440	$\min_{\mathbf{Z}} \frac{\rho_k}{2} \ \mathbf{Z}\ _F^2 + \ \mathbf{Z}\ _{w,*}$	494
441	3. Update $\mathbf{A}_{k+1}$ as $\mathbf{A}_{k+1} = \mathbf{A}_k + \rho_k (\mathbf{X}_{k+1} - \mathbf{Z}_{k+1})$	495
442	4. Update $\rho_{k+1} = \mu * \rho_k$ ;	496
443	5. $k \leftarrow k + 1$ ;	497
444	<b>if</b> (Convergence conditions are satisfied) or ( $k \geq K_2$ )	498
445	5. $\text{T} \leftarrow \text{True}$	499
446	<b>end if</b>	500
447	<b>end while</b>	501
448	<b>Output:</b> Matrices $\mathbf{X}$ and $\mathbf{Z}$ .	502

*Proof.* We give proof sketch here and detailed proof of this theorem can be found in supplementary files. We can first proof that the sequence  $\{\mathbf{A}_k\}$  generated by Algorithm 3.4 is upper bounded. Since  $\{\rho_k\}$  is unbounded, that is  $\lim_{k \rightarrow \infty} \rho_k = +\infty$ , we can proof that the sequence of Lagrangian function  $\{\mathcal{L}(\mathbf{X}_{k+1}, \mathbf{Z}_{k+1}, \mathbf{A}_k, \rho_k)\}$  is also upper bounded. Hence, both  $\{\mathbf{W}(\mathbf{Y} - \mathbf{X}_k)\}$  and  $\{\mathbf{Z}_k\}$  are upper bounded. According to Eq. (18), we can proof that  $\lim_{k \rightarrow \infty} \|\mathbf{X}_{k+1} - \mathbf{Z}_{k+1}\|_F = \lim_{k \rightarrow \infty} \rho_k^{-1} \|\mathbf{A}_{k+1} - \mathbf{A}_k\|_F = 0$ , and (a) is proofed. Then we can proof that  $\lim_{k \rightarrow \infty} \|\mathbf{X}_{k+1} - \mathbf{X}_k\|_F \leq \lim_{k \rightarrow \infty} \|(\mathbf{W}^\top \mathbf{W} + \frac{\rho_k}{2} \mathbf{I})^{-1} (\mathbf{W}^\top \mathbf{W} \mathbf{Y} - \mathbf{W}^\top \mathbf{W} \mathbf{Z}_k - \frac{1}{2} \mathbf{A}_k)\|_F + \rho_k^{-1} \|\mathbf{A}_k - \mathbf{A}_{k-1}\|_F = 0$  and hence (b) is proofed. Then (c) can be proofed by checking that  $\lim_{k \rightarrow \infty} \|\mathbf{Z}_{k+1} - \mathbf{Z}_k\| \leq \lim_{k \rightarrow \infty} \|\Sigma_{k-1} - \mathcal{S}_{w/\rho_{k-1}}(\Sigma_{k-1})\|_F + \|\mathbf{X}_{k+1} - \mathbf{X}_k\|_F + \rho_k^{-1} \|\mathbf{A}_{k-1} + \mathbf{A}_{k+1} - \mathbf{A}_k\|_F = 0$ , where  $\mathbf{U}_{k-1} \Sigma_{k-1} \mathbf{V}_{k-1}^\top$  is the SVD of the matrix  $\mathbf{X}_k + \rho_{k-1} \mathbf{A}_{k-1}$ .  $\square$

## 4. Experiments

We evaluate the proposed MC-WNNM method on synthetic and real color image denoising. We compare the proposed method with other state-of-the-art denoising methods including CBM3D [15], MLP [10], WNNM [7], TNRD [12], “Noise Clinic” (NC) [17, 25], and the commercial software Neat Image (NI) [27].

### 4.1. Implementation Details

In synthetic experiments, the noise levels in R, G, B channels are assumed to be known as  $\sigma_r, \sigma_g, \sigma_b$ . In the real cases, the noise levels in R, G, B channels can be estimated via noise estimation methods [28, 29]. In this paper, we employ the method of [29] for its state-of-the-art performance. For the CBM3D method [15], the input noise levels are the Root Mean Square (RMS) as

$$\sigma = \sqrt{(\sigma_r^2 + \sigma_g^2 + \sigma_b^2)/3}. \quad (22)$$

For the methods of MLP [10] and TNRD [12], we retrain the models on grayscale images following their corresponding strategies at different noise levels from  $\sigma = 5$  to  $\sigma = 75$  with gap of 5. The denoising on color images is performed by processing separately each channel with the model trained at the same (or nearest) noise levels. NC [17, 25] is a blind image denoising method, so we just submit the noisy images (synthetic or real) to [25] and perform denoising using the default parameters. NI [27] is a commercial software suitable for real image denoising, while the code of CC [18] is not released (but its results on the 15 real noisy images in [18] are available by requesting the authors). Hence, we only compare with CC and NI in real image denoising experiments, and do not compare with them in synthetic experiments.

In order to take fully comparison with the original WNNM method [23], we extended the WNNM method [23] for color image denoising in three directions: 1) we apply the WNNM method [23] on each channel separately with corresponding noise levels  $\sigma_r, \sigma_g, \sigma_b$ . We call this method “WNNM0”; 2) we perform denoising on the joint vectors concatenated by corresponding patches in the R, G, B channels, where the input noise level  $\sigma$  is computed by RMS (Eq. (22)). We call this method “WNNM1”; 3) we set the weighting matrix  $\mathbf{W}$  in the proposed MC-WNNM model as  $\mathbf{W} = \sigma^{-1} \mathbf{I}$ . For fair comparison, we tune all these methods set the same parameters for “WNNM2” and the proposed MC-WNNM methods while achieving the best performance of “WNNM2”. For fair comparison, we tune the methods of “WNNM0”, “WNNM1”, “WNNM2”, and the proposed MC-WNNM to achieve corresponding best denoising performance (i.e., highest average PSNR results).

### 4.2. Experiments on Synthetic Noisy Images

In this section, we compare the proposed MC-WNNM method with other competing method [10, 12, 15, 17, 27] as well as the three extensions of WNNM [23] on the 24 high quality color images from the Kodak PhotoCD Dataset (<http://r0k.us/graphics/kodak/>), which are shown in Fig. 2. The noisy images are generated by adding additive white Gaussian noise (AWGN) with known standard derivations  $\sigma_r, \sigma_g, \sigma_b$  for the R, G, B channels, respectively. In this paper, the noise levels we add to each channel of the 24 color images are  $\sigma_r = 40, \sigma_g = 20, \sigma_b = 30$ , respectively. More experiments can be found in the supplementary files. For the methods of “WNNM2” and MC-WNNM, we set the patch size as  $p = 6$ , the number of non-local similar patches as  $M = 70$ , the window size for searching similar patches as  $W = 20$ , the updating parameter  $\mu = 1.001$ , the number of iterations in Algorithm 1 as  $K_1 = 8$ , the number of iterations in Algorithm 2 as  $K_2 = 10$ . For “WNNM2”, the initial penalty parameter is set as  $\rho_0 = 10$ , while for the



540  
541  
542  
543  
544  
545  
546  
547  
548  
549  
550  
551  
552  
553  
554  
555  
556  
557  
558  
559  
560  
561  
562  
563  
564  
565  
566  
567  
568  
569  
570  
571  
572  
573  
574  
575  
576  
577  
578  
579  
580  
581  
582  
583  
584  
585  
586  
587  
588  
589  
590  
591  
592  
593  
Figure 2. The 24 high quality color images from the Kodak PhotoCD Dataset.

proposed MC-WNNM model, the penalty parameter is set as  $\rho_0 = 3$ .

The PSNR results are listed in Table 1 of the compared methods including CBM3D [15], MLP [10], TNRD [12], NC [17, 25], “WNNM0” [23], “WNNM1”, “WNNM2” and the proposed MC-WNNM methods. The best PSNR results are highlighted in bold. One can see that on all the 24 images, our method achieves the highest PSNR values over the competing methods. On average PSNR, our proposed method achieves 0.48dB improvements over the “WNNM0” method and outperforms the “WNNM2” by 1.09dB. Fig. 3 shows a scene denoised by the compared methods. We can see that CBM3D and NC would remain noise while MLP and TNRD would generate artifacts. The methods of “WNNM0”, “WNNM1”, “WNNM2” would over-smooth much the image. By using the proposed MC-WNNM model, our method preserves the structures (e.g., edges and textures) better across the R, G, B channels and generate less artifacts than other denoising methods, leading to visually pleasant outputs. More visual comparisons can be found in the supplementary files.

#### 4.3. Experiments on Real Noisy Images

In this section, we compare the proposed MC-WNNM method with other competing methods on the 15 real noisy images (Fig. 4). We do not compare with the “WNNM0” method due to limited space and its inferior performance. The noisy images were collected under controlled indoor environment. Each scene was shot 500 times under the same camera and camera setting. The mean image of the 500 shots is roughly taken as the “ground truth”, with which the PSNR can be computed. Since the image size is very large (about  $7000 \times 5000$ ) and the 11 scenes share repetitive contents, the authors of [18] cropped 15 smaller images (of size  $512 \times 512$ ) to perform experiments. For each real noisy image, the noise levels in R, G, B channels are estimated by [29]. Since the noise levels are small in real noisy images, for the method of MLP [10] and TNRD [12], we apply the trained models of corresponding methods and choose the best denoising results (highest average PSNR values). Both methods achieves best results when setting the noise levels

of the trained models from  $\sigma = 10$ .

We perform quantitative comparison on the 15 cropped images used in [18]. The PSNR results are listed in Table 2 of the compared methods including CBM3D [15], MLP [10], TNRD [12], NC [17, 25], NI [27], CC [18] (copied from [18]), “WNNM1”, “WNNM2”, and the proposed MC-WNNM method. The highest PSNR results are highlighted in bold. On average PSNR, the proposed MC-WNNM method achieves 0.44dB improvements over the “WNNM1” method and outperforms the state-of-the-art denoising method CC [18] by 0.83dB. On 10 out of the whole 15 images, the proposed MC-WNNM method achieves the highest PSNR values. Both CC and “WNNM1” achieves highest PSNR results on 2 of 15 images. It should be noted that in the CC method, a specific model is trained for each camera and camera setting, while our method uses the same model for all images. Fig. 5 shows the denoised images of a scene captured by Canon 5D Mark 3 at ISO = 3200. We can see that CBM3D, NC, NI and CC would either remain noise or generate artifacts, while MLP, TNRD over-smooth much the image. By using the proposed MC-WNNM model achieves better visual quality results than other methods. More visual comparisons can be found in the supplementary files.

## 5. Conclusion and Future Work

The real noisy images have different noise structures among the R, G, B channels due to the preprocessing steps of the in-camera imaging pipelines in CCD or CMOS sensors. This makes the real image denoising problem much more complex than grayscale image denoising. In this paper, we proposed a novel multi-channel (MC) model for real color image denoising. By introducing a weighting matrix to the concatenated weighted nuclear norm minimization (WNNM) model, the proposed MC-WNNM model can process adaptively the different noise structures in each of the R, G, B channels and exploit the non-local self similarity property of natural images. Though no longer having closed-form solution, we successfully solved the MC-WNNM model via an ADMM algorithm by reformulating the MC-WNNM model as a linear equality-constrained problem with two separable variables. We also studied the convergence property of the ADMM algorithm. Extensive experiments on synthetic and real color image denoising demonstrate that, the proposed MC-WNNM model outperforms the other competing denoising methods on both synthetic color noisy images as well as real-world noisy images. The introduce of the weighting matrix can boost the performance of traditional models on new applications. We believe that this work can be extended in at least two directions. Firstly, the weighting matrix beyond the diagonal form, such as correlation form [30], may bring better performance on color image denoising. Secondly, the proposed

594  
595  
596  
597  
598  
599  
600  
601  
602  
603  
604  
605  
606  
607  
608  
609  
610  
611  
612  
613  
614  
615  
616  
617  
618  
619  
620  
621  
622  
623  
624  
625  
626  
627  
628  
629  
630  
631  
632  
633  
634  
635  
636  
637  
638  
639  
640  
641  
642  
643  
644  
645  
646  
647

Table 1. PSNR(dB) results of different denoising algorithms on 24 natural images.

Image#	CBM3D	MLP	TNRD	NI	NC	WNNM0	WNNM1	WNNM2	MC-WNNM
$\sigma_r = 40, \sigma_g = 20, \sigma_b = 30$									
1	25.24	25.70	25.74	23.85	24.90	26.01	25.95	25.58	<b>26.66</b>
2	28.27	30.12	30.21	25.90	25.87	30.08	30.11	29.80	<b>30.20</b>
3	28.81	31.19	31.49	26.00	28.58	31.58	31.61	31.20	<b>32.25</b>
4	27.95	29.88	29.86	25.82	25.67	30.13	30.16	29.84	<b>30.49</b>
5	25.03	26.00	26.18	24.38	25.15	26.44	26.39	25.32	<b>26.82</b>
6	26.24	26.84	26.90	24.65	24.74	27.39	27.30	26.88	<b>27.98</b>
7	27.88	30.28	30.40	25.63	27.69	30.47	30.54	29.70	<b>30.98</b>
8	25.05	25.59	25.83	24.02	25.30	26.71	26.75	25.26	<b>26.90</b>
9	28.44	30.75	30.81	25.94	27.44	30.86	30.92	30.29	<b>31.49</b>
10	28.27	30.38	30.57	25.87	28.42	30.65	30.68	29.95	<b>31.26</b>
11	26.95	28.00	28.14	25.32	24.67	28.19	28.16	27.61	<b>28.63</b>
12	28.76	30.87	31.05	26.01	28.37	30.97	31.06	30.58	<b>31.48</b>
13	23.76	23.95	23.99	23.53	22.76	24.27	24.15	23.52	<b>24.89</b>
14	26.02	26.97	27.11	24.94	25.68	27.20	27.15	26.55	<b>27.57</b>
15	28.38	30.15	30.44	26.06	28.21	30.52	30.60	30.13	<b>30.81</b>
16	27.75	28.82	28.87	25.69	26.66	29.27	29.21	29.02	<b>29.96</b>
17	27.90	29.57	29.80	25.85	28.32	29.78	29.79	29.16	<b>30.40</b>
18	25.77	26.40	26.41	24.74	25.70	26.63	26.56	26.01	<b>27.22</b>
19	27.30	28.67	28.81	25.40	26.52	29.19	29.22	28.67	<b>29.57</b>
20	28.96	30.40	30.76	24.95	25.90	30.79	30.83	29.97	<b>31.07</b>
21	26.54	27.53	27.60	25.06	26.48	27.80	27.75	27.12	<b>28.34</b>
22	27.05	28.17	28.27	25.36	26.60	28.21	28.16	27.81	<b>28.64</b>
23	29.14	32.31	32.51	26.13	23.24	31.89	31.97	31.21	<b>32.34</b>
24	25.75	26.41	26.53	24.55	25.73	27.10	27.03	26.18	<b>27.59</b>
Average	27.13	28.54	28.68	25.24	26.19	28.84	28.83	28.22	<b>29.31</b>

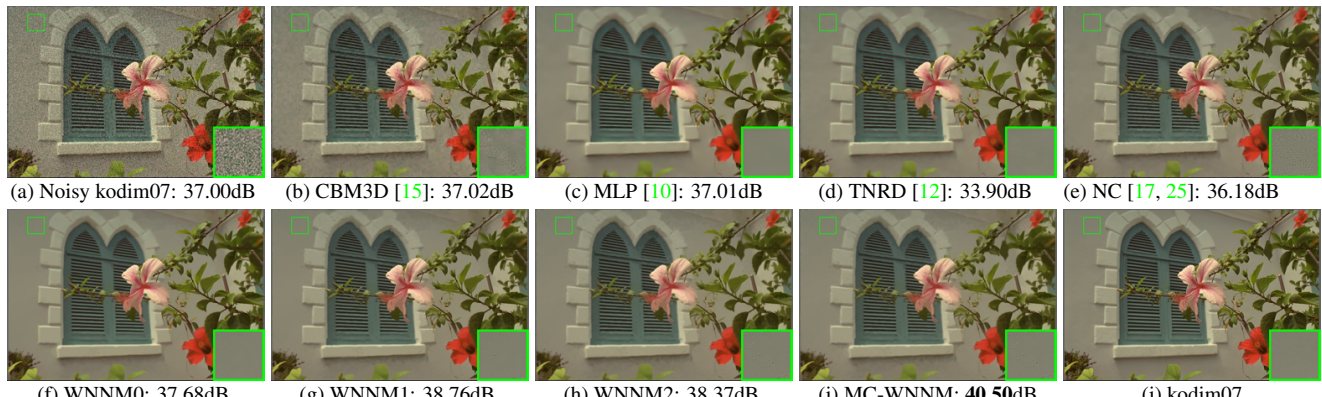


Figure 3. Denoised images of different methods on the image “kodim07” degraded by noise with different levels on different channels. The images are better to be zoomed in on screen.

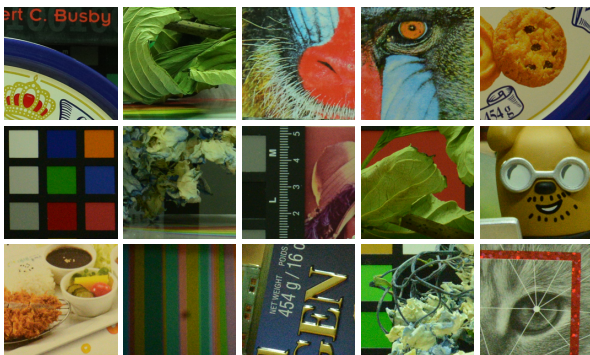


Figure 4. The 15 cropped real noisy images used in [18].

MC-WNNM model can be further extended to deal with hyperspectral images, which contain much more channels than color images.

## References

- [1] A. Buades, B. Coll, and J. M. Morel. A non-local algorithm for image denoising. *IEEE Conference on Computer Vision and Pattern Recognition (CVPR)*, pages 60–65, 2005. **1**
- [2] K. Dabov, A. Foi, V. Katkovnik, and K. Egiazarian. Image denoising by sparse 3-D transform-domain collaborative filtering. *IEEE Transactions on Image Processing*, 16(8):2080–2095, 2007. **1, 2, 7, 8**
- [3] M. Elad and M. Aharon. Image denoising via sparse and redundant representations over learned dictionaries. *IEEE Transactions on Image Processing*, 15(12):3736–3745, 2006.
- [4] J. Mairal, F. Bach, J. Ponce, G. Sapiro, and A. Zisserman. Non-local sparse models for image restoration. *IEEE International Conference on Computer Vision (ICCV)*, pages 2272–2279, 2009.

Table 2. PSNR(dB) results of different methods on 15 cropped real noisy images used in [18].

Camera Settings	CBM3D	MLP	TNRD	NI	NC	CC	WNNM1	WNNM2	MC-WNNM
Canon 5D Mark III ISO = 3200	39.76	39.00	39.51	35.68	36.20	38.37	39.74	39.98	<b>41.13</b>
	36.40	36.34	36.47	34.03	34.35	35.37	35.12	36.65	<b>37.28</b>
	36.37	36.33	36.45	32.63	33.10	34.91	33.14	34.63	<b>36.52</b>
Nikon D600 ISO = 3200	34.18	34.70	34.79	31.78	32.28	34.98	35.08	35.08	<b>35.53</b>
	35.07	36.20	36.37	35.16	35.34	35.95	36.42	36.84	<b>37.02</b>
	37.13	39.33	39.49	39.98	40.51	<b>41.15</b>	40.78	39.24	39.56
Nikon D800 ISO = 1600	36.81	37.95	38.11	34.84	35.09	37.99	38.28	38.61	<b>39.26</b>
	37.76	40.23	40.52	38.42	38.65	40.36	41.24	40.81	<b>41.43</b>
	37.51	37.94	38.17	35.79	35.85	38.30	38.04	38.96	<b>39.55</b>
Nikon D800 ISO = 3200	35.05	37.55	37.69	38.36	38.56	<b>39.01</b>	39.93	37.97	38.91
	34.07	35.91	35.90	35.53	35.76	36.75	37.32	37.30	<b>37.41</b>
	34.42	38.15	38.21	40.05	40.59	39.06	<b>41.52</b>	38.68	39.39
Nikon D800 ISO = 6400	31.13	32.69	32.81	34.08	34.25	34.61	<b>35.20</b>	34.57	34.80
	31.22	32.33	32.33	32.13	32.38	33.21	33.61	33.43	<b>33.95</b>
	30.97	32.29	32.29	31.52	31.76	33.22	33.62	<b>34.02</b>	33.94
Average	35.19	36.46	36.61	35.33	35.65	36.88	37.27	37.12	<b>37.71</b>

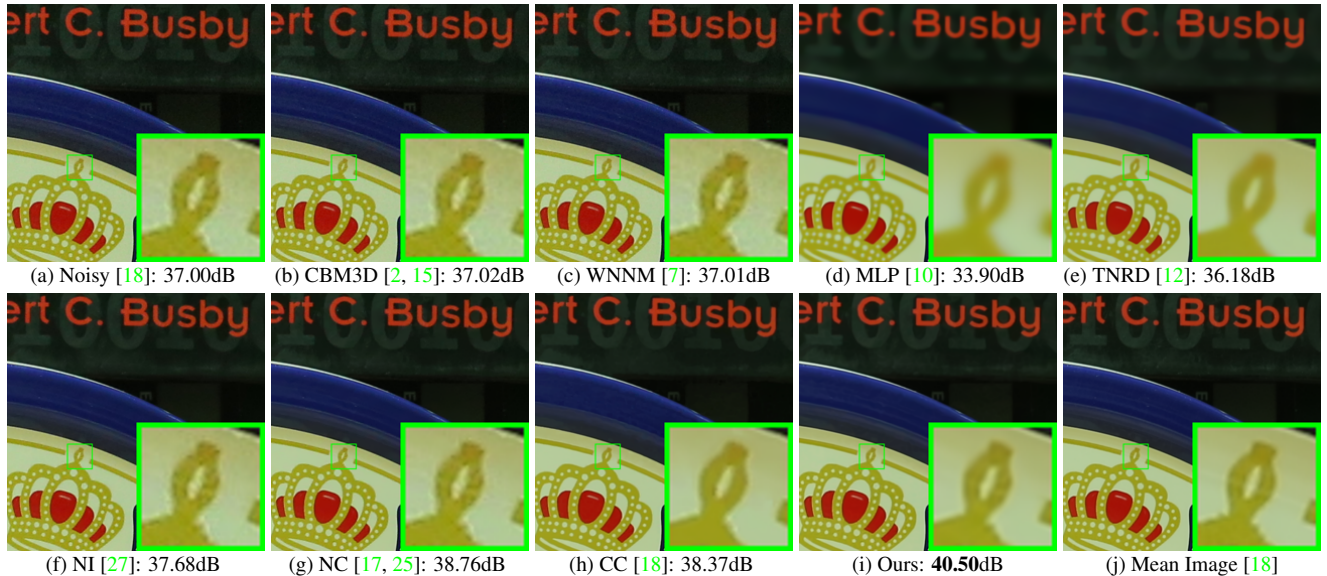


Figure 5. Denoised images of a region cropped from the real noisy image “Canon 5D Mark 3 ISO 3200 1” [18] by different methods. The images are better to be zoomed in on screen.

[5] W. Dong, L. Zhang, G. Shi, and X. Li. Nonlocally centralized sparse representation for image restoration. *IEEE Transactions on Image Processing*, 22(4):1620–1630, 2013.

[6] J. Xu, L. Zhang, W. Zuo, D. Zhang, and X. Feng. Patch group based nonlocal self-similarity prior learning for image denoising. *IEEE International Conference on Computer Vision (ICCV)*, pages 244–252, 2015.

[7] S. Gu, L. Zhang, W. Zuo, and X. Feng. Weighted nuclear norm minimization with application to image denois-

ing. *IEEE Conference on Computer Vision and Pattern Recognition (CVPR)*, pages 2862–2869, 2014. 1, 2, 5, 8

[8] S. Roth and M. J. Black. Fields of experts. *International Journal of Computer Vision*, 82(2):205–229, 2009. 1

[9] D. Zoran and Y. Weiss. From learning models of natural image patches to whole image restoration. *IEEE International Conference on Computer Vision (ICCV)*, pages 479–486, 2011.

[10] H. C. Burger, C. J. Schuler, and S. Harmeling. Image denoising: Can plain neural networks compete with BM3D?

- 864      IEEE Conference on Computer Vision and Pattern Recognition (CVPR), pages 2392–2399, 2012. 5, 6, 7, 8      918
- 865      919
- 866      920
- 867      [11] U. Schmidt and S. Roth. Shrinkage fields for effective im-      921
- 868      age restoration. *IEEE Conference on Computer Vision and*      922
- 869      *Pattern Recognition (CVPR)*, pages 2774–2781, June 2014.      923
- 870      924
- 871      925
- 872      [12] Y. Chen, W. Yu, and T. Pock. On learning optimized re-      926
- 873      action diffusion processes for effective image restoration.      927
- 874      *IEEE Conference on Computer Vision and Pattern Recog-*      928
- 875      *nition (CVPR)*, pages 5261–5269, 2015. 1, 5, 6, 7, 8      929
- 876      930
- 877      [13] H. C. Karaimer and M. S. Brown. A software platform for      931
- 878      manipulating the camera imaging pipeline. *European Con-*      932
- 879      *ference on Computer Vision (ECCV)*, October 2016. 1, 2      933
- 880      934
- 881      [14] Julien Mairal, Michael Elad, and Guillermo Sapiro. Sparse      935
- 882      representation for color image restoration. *IEEE Transac-*      936
- 883      *tions on Image Processing*, 17(1):53–69, 2008. 1, 2      937
- 884      938
- 885      [15] K. Dabov, A. Foi, V. Katkovnik, and K. Egiazarian. Color      939
- 886      image denoising via sparse 3D collaborative filtering with      940
- 887      grouping constraint in luminance-chrominance space. *IEEE*      941
- 888      *International Conference on Image Processing (ICIP)*, pages      942
- 889      313–316, 2007. 1, 2, 5, 6, 7, 8      943
- 890      944
- 891      945
- 892      [16] C. Liu, R. Szeliski, S. Bing Kang, C. L. Zitnick, and W. T.      946
- 893      Freeman. Automatic estimation and removal of noise from      947
- 894      a single image. *IEEE Transactions on Pattern Analysis and*      948
- 895      *Machine Intelligence*, 30(2):299–314, 2008. 1, 2      949
- 896      950
- 897      [17] M. Lebrun, M. Colom, and J.-M. Morel. Multiscale image      951
- 898      blind denoising. *IEEE Transactions on Image Processing*,      952
- 899      24(10):3149–3161, 2015. 2, 5, 6, 7, 8      953
- 900      954
- 901      [18] S. Nam, Y. Hwang, Y. Matsushita, and S. J. Kim. A holistic      955
- 902      approach to cross-channel image noise modeling and its ap-      956
- 903      plication to image denoising. *IEEE Conference on Computer*      957
- 904      *Vision and Pattern Recognition (CVPR)*, pages 1683–1691,      958
- 905      2016. 1, 2, 5, 6, 7, 8      959
- 906      960
- 907      961
- 908      [19] F. Zhu, G. Chen, and P.-A. Heng. From noise modeling to      962
- 909      blind image denoising. *IEEE Conference on Computer Vi-*      963
- 910      *sion and Pattern Recognition (CVPR)*, June 2016. 1, 2      964
- 911      965
- 912      [20] S. Boyd, N. Parikh, E. Chu, B. Peleato, and J. Eckstein. Dis-      966
- 913      tributed optimization and statistical learning via the alternat-      967
- 914      ing direction method of multipliers. *Found. Trends Mach.*      968
- 915      *Learn.*, 3(1):1–122, January 2011. 1      969
- 916      970
- 917      971
- [21] C. Lu, C. Zhu, C. Xu, S. Yan, and Z. Lin. Generalized sin-      962
- 918      gular value thresholding. *AAAI*, 2015. 1      963
- [22] J. Cai, E. J. Candès, and Z. Shen. A singular value thresh-      964
- 919      olding algorithm for matrix completion. *SIAM Journal on*      965
- 920      *Optimization*, 20(4):1956–1982, 2010. 2      966
- [23] S. Gu, Q. Xie, D. Meng, W. Zuo, X. Feng, and L. Zhang.      967
- 921      Weighted nuclear norm minimization and its applications to      968
- 922      low level vision. *International Journal of Computer Vision*,      969
- 923      pages 1–26, 2016. 2, 3, 4, 5, 6      970
- 924      971
- [24] C. Eckart and G. Young. The approximation of one matrix by      972
- 925      another of lower rank. *Psychometrika*, 1(3):211–218, 1936.      973
- [25] M. Lebrun, M. Colom, and J. M. Morel. The noise clinic:      974
- 926      a blind image denoising algorithm. [http://www.ipol.](http://www.ipol.im/pub/art/2015/125/)      975
- 927      im/pub/art/2015/125/. Accessed 01 28, 2015. 2, 5,      976
- 928      6, 7, 8      977
- [26] C. Kervrann, J. Boulanger, and P. Coupé. Bayesian non-      978
- 929      local means filter, image redundancy and adaptive dictionar-      979
- 930      ies for noise removal. *International Conference on Scale*      980
- 931      *Space and Variational Methods in Computer Vision*, pages      981
- 932      520–532, 2007. 2      982
- [27] Neatlab ABSoft. Neat Image. [https://ni.](https://ni.neatvideo.com/home)      983
- 933      neatvideo.com/home. 2, 5, 6, 8      984
- [28] X. Liu, M. Tanaka, and M. Okutomi. Single-image noise      985
- 934      level estimation for blind denoising. *IEEE Transactions on*      986
- 935      *Image Processing*, 22(12):5226–5237, 2013. 5      987
- [29] G. Chen, F. Zhu, and A. H. Pheng. An efficient statistical      988
- 936      method for image noise level estimation. *IEEE International*      989
- 937      *Conference on Computer Vision (ICCV)*, December 2015. 5,      990
- 938      6      991
- [30] N. J. Higham. Computing the nearest correlation matrixa      992
- 939      problem from finance. *IMA Journal of Numerical Analysis*,      993
- 940      22(3):329, 2002. 6      994
- 941      995
- 942      996
- 943      997
- 944      998
- 945      999
- 946      1000
- 947      1001
- 948      1002
- 949      1003
- 950      1004
- 951      1005
- 952      1006
- 953      1007
- 954      1008
- 955      1009
- 956      1010
- 957      1011
- 958      1012
- 959      1013
- 960      1014
- 961      1015
- 962      1016
- 963      1017
- 964      1018
- 965      1019
- 966      1020
- 967      1021
- 968      1022
- 969      1023
- 970      1024
- 971      1025